The phase-space structure of a dark-matter halo: Implications for dark-matter direct detection experiments

Amina Helmi, Simon D.M. White and Volker Springel*
Max-Planck-Institut für Astrophysik, Karl-Schwarzschild-Str. 1, 85740 Garching bei München, Germany
(Dated: July 23, 2002)

We study the phase-space structure of a dark-matter halo formed in a high resolution simulation of a ΛCDM cosmology. Our goal is to quantify how much substructure is left over from the inhomogeneous growth of the halo, and how it may affect the signal in experiments aimed at detecting the dark matter particles directly. If we focus on the equivalent of "Solar vicinity", we find that the dark-matter is smoothly distributed in space. The probability of detecting particles bound within dense lumps of individual mass less than $10^7 M_\odot h^{-1}$ is small, less than 10^{-2}. The velocity ellipsoid in the Solar neighbourhood deviates only slightly from a multivariate Gaussian, and can be thought of as a superposition of thousands of kinematically cold streams. The motions of the most energetic particles are, however, strongly clumped and highly anisotropic. We conclude that experiments may safely assume a smooth multivariate Gaussian distribution to represent the kinematics of dark-matter particles in the Solar neighbourhood. Experiments sensitive to the direction of motion of the incident particles could exploit the expected anisotropy to learn about the recent merging history of our Galaxy.

PACS numbers: 95.35.+d,95.30.Cq,95.75.Pq,98.35.Gi,98.35.Df,98.35.Mp

I. INTRODUCTION

One of the most fundamental open questions in cosmology and particle physics today is what is the nature of dark-matter. The first indications of its existence came in the 1930s, with the measurements of the velocities of galaxies in clusters. The cluster mass required to gravitationally bind the galaxies was found to be roughly an order of magnitude larger than the sum of the luminous masses of the individual galaxies [1, 2]. In the 1970s, observations of the rotation curves of spiral galaxies ($V_c(r) = \sqrt{GM(r)/r}$) showed that these were flat or even rising at distances far beyond their stellar and gaseous components [3–5]. These discoveries led to the conclusion that a large fraction (more than 90%) of the mass in the Universe is dark. It is now widely believed that this mass is most likely in the form of yet to be discovered nonbaryonic elementary particles.

Being the dominant mass component of galaxies and of large-scale structures in the Universe, dark-matter has necessarily become a key ingredient in theories of structure formation in the Universe. The most successful of these theories is the hierarchical paradigm [6]. In the current (and observationally most favoured) version of this model, the nonbaryonic elementary particles are known as "cold dark-matter" (CDM) [7]. The term "cold" derives from the fact that the dark-matter particles had non-relativistic motions at the time of matter–radiation equality. Their abundance was set when the interaction rate became too small for the particles to be in thermal equilibrium in the expanding Universe.

*Electronic address: ahelmi,swhite,volker@mpa-garching.mpg.de

The first objects to form in a CDM Universe are small galaxies, which then merge and give rise to the larger scale structures we observe today. Thus structure formation occurs in a "bottom-up" fashion [8, 9]. This hierarchical paradigm has allowed astronomers to make very definite predictions for the properties of galaxies today and about their evolution from high redshift. Direct comparisons to observations have shown that this model is quite successful in reproducing both the local and the distant Universe.

The crucial test of this paradigm undoubtedly consists in the determination of the nature of dark-matter through direct detection experiments. Among the most promising candidates from the particle physics perspective are axions and neutralinos. Axions have been introduced to solve the strong-CP (Charge conjugation and Parity) violations [10]. They can be detected through their conversion to photons in the presence of a strong magnetic field (e.g. [11, 12]). Neutralinos are the lightest supersymmetric particles, and may be considered as a particular form of weakly interacting massive particles (WIMPs). The most important direct detection process of neutralinos is through elastic scattering on nuclei. The idea is to determine the count rate over recoil energy above a given (detector) background level. The experimental situation has been improving rapidly over the past years, with large-scale collaborations such as DAMA, Edelweiss and CDMS [13–15] starting to probe interesting regions of parameter space (for an extensive discussion see [16]). The main problem currently lies in the high level of background noise, either from ambient radioactivity or cosmic-ray induced activity. Information on the direction of the recoils could potentially also be useful and yield a large improvement in sensitivity [17].

In all these experiments, the count rate strongly depends on the velocity distribution of the incident particles, and a modulation effect due to the orbital motion of the Earth around the Sun is expected [18]. In most cases, an isotropic Maxwellian distribution has been assumed (e.g. [19, 20]), although there are other examples in the recent literature, discussing multivariate Gaussian distributions [21–23]. Attempts at understanding the effect of substructure in the velocity distribution of dark-matter particles have also been made [24–26]. This substructure would have its origin in the different merger and accretion events the Galaxy should have experienced over its lifetime [27].

The progressive build up of dark halos through mergers and accretion of smaller subunits implies that the latter will leave substructure in the phase-space of the final object. This is because the phase-space volume of the final object is much larger than that initially available for each one of the objects independently. For example, for a small satellite galaxy the initial phase-space volume occupied by its particles is proportional to $(R^{\rm sat} V_c^{\rm sat})^3$, where $R^{\rm sat}$ is the size of the satellite, and $V_c^{\rm sat}$ its circular velocity. The volume available to the satellite particles after the merging is determined by their orbit, and is a factor $(R^{\rm gal}/R^{\rm sat})^3 \times (V_c^{\rm gal}/V_c^{\rm sat})^3$ larger, where $R^{\rm gal}$ is the size of the final object and $V_c^{\rm gal}$ its circular velocity. Note that even in the case of a major merger, where the mass is doubled, the phase-space volume available is already 4 times larger [45]. The key question is whether this substructure will be directly or indirectly observable. For example, if there is a bound satellite going through the Solar neighbourhood at the present day, it will dominate the flux of dark-matter particles on Earth. The energy spectrum of these particles will be strongly peaked around the orbital energy of the clump, perhaps giving a signal similar to a delta function. As we shall show in Sec.III B 2 the fraction of mass in satellites which could have survived the tidal field of the Galaxy by the present day is less than 10^{-2} of total mass of the Galaxy, implying that such a scenario is relatively unlikely.

More realistic is to assume that the satellite halos that contribute with mass to the Solar neighbourhood will be completely disrupted. The particles freed from such satellites will tend to follow the initial orbit of their progenitor, and eventually will fill a volume comparable to the size of the orbit. Because of the conservation of phase-space density (Liouville's theorem), this implies that locally they should have very similar velocities [46]. Thus one may expect to see streams of particles going through the Solar neighbourhood, which had their origin in the different merging events. Such streams have already been observed in the motions of nearby halo stars and in the outer regions of the Galactic halo [28, 29]. Streams manifest themselves as peaks in the velocity distribution function. Clearly it is important to determine for the dark-matter particles in the vicinity of the Sun whether this distribution function will be dominated by a few of these peaks, or whether their number is so large, that it will be close to Gaussian.

The best way to understand the expected properties of the Galactic halo in the Solar neighbourhood is through high-resolution simulations starting from appropriate cosmological initial conditions. Analytic modelling can provide insights into the processes that drive the build-up of structure such as phase-mixing, or tidal stripping. Nevertheless it needs to be complemented by cosmological simulations, that provide the mass spectrum of the accreted halos, their orbital parameters, their characteristic merging times, and the detailed mixing of the material they deposit. The highly non-linear character of the hierarchical build up of a galaxy like the Milky Way, forces us to resort to numerical simulations to make realistic predictions for its properties. Very high resolution simulations are required to be able to resolve the substructures leftover from merging events, since their density contrasts are expected to fade rather quickly with time (as t^3 for sufficiently long timescales [27]).

The main goal of the present paper is to understand the phase-space structure of a dark-matter halo. We wish to quantify the expected amount of substructure and understand its effect on direct dark-matter detection experiments. Particular emphasis will be put on determining the properties of the dark-matter distribution in the Solar neighbourhood: its mass growth history, the spatial distribution and the kinematics of particles in this region of the Galactic halo. We address these issues by scaling down a high-resolution simulation of the formation of a cluster of galaxies in a ΛCDM cosmology to a galactic size halo [30].

II. METHODOLOGY

The simulations we analyse here were carried out using a parallel tree-code [31] on the Cray T3E at the Garching Computing Centre of the Max Planck Society. These simulations were generated by zooming in and re-simulating with higher resolution a particular cluster and its surroundings formed in a cosmological simulation (as in [32]). The ΛCDM cosmological simulation has parameters $\Omega_0 = 0.3$, $\Omega_\Lambda = 0.7$, $h = 0.7$ and $\sigma_8 = 0.9$. The cluster selected is the second most massive cluster in the simulation and has a virial mass of $8.4 \times 10^{14} h^{-1}\,{\rm M}_\odot$. The particles that end up in the final cluster of the cosmological simulation and in its immediate surroundings (defined by a comoving sphere of $70h^{-1}$ Mpc radius) were traced back to their Lagrangian region in the initial conditions for re-simulation. The initial mass distribution between 21 and $70h^{-1}$ Mpc was represented by 3×10^6 particles. In the inner region, where the original simulation had 2.2×10^5 particles, new initial conditions were created for 4.5×10^5, 2×10^6, 1.3×10^7 and 6.6×10^7 particles, and small scale power was also added onto this volume. The original force softening was also decreased to obtain better spatial resolution. All simulations were run from very high redshift until $z = 0$.

We can scale the simulated cluster to a "Milky Way" halo by scaling the circular velocity so that at its maximum it is equal to 220 km s^{-1}. The scaling factor obtained in this case is $\gamma = v_c^{cl}/v_c^{MW} \sim 9.18$. The virial radius of our simulated "Milky Way" dark-matter halo is $r_{\rm vir} = 228$ kpc. The justification for this simple scaling relies both on theoretical and numerical results [34–36]. For example, high-resolution numerical simulations have shown that the overall properties of galaxies and clusters of galaxies, such as their density profiles, number of satellites and formation paths have overlapping statistical distributions for the two types of objects.

III. THE PHASE-SPACE STRUCTURE OF THE GALAXY

In this section we shall focus on the properties of the dark-matter distribution, with particular emphasis on the vicinity of the "Sun". We are interested in which halos contribute matter to this region of the Galactic halo, what were their initial properties, and when were they accreted. We also investigate what is the present-day spatial and velocity distribution of material in the "Solar neighbourhood", and how the direct detection experiments may be fine tuned to determine the nature of dark-matter.

A series of snapshots of the growth of the cluster are shown in Figure 1. The simulations start from very small density fluctuations, assumed to have been produced during the inflationary expansion of the Universe [33]. Matter is then accreted onto these initial density fluctuations through the action of gravity. A dark halo forms when an overdense region decouples from the expanding Universe, turns around and collapses onto itself. This process repeats itself on progressively larger scales, and big halos are formed through the merging and accretion of smaller units as shown in Fig. 1. These subunits will orbit the larger halo as satellites for some time, as shown in the bottom panels in Fig. 1, until they are completely disrupted. We will frequently refer to them as subhalos. The progressive growth of mass of the cluster is schematically shown in Figure 2 as a "merger tree".

A. Mass growth history

1. The Galaxy

Let us first study the properties of the dark-matter distribution as a function of distance from the galaxy centre. We are interested in determining what type of halos typically contribute to different regions of the galaxy and their time of accretion. This is relevant because halos accreted at late times will be generally less mixed, and could thus produce more massive streams dominating the velocity distribution of particles near the Sun. We also want to estimate the probability that such halos could contribute to the Solar neighbourhood mass budget.

We proceed by dividing the halo in six spherical shells around the galaxy centre. These shells are located at: $r < 10$ kpc, $10 \leq r < 25$ kpc, $25 \leq r < 50$ kpc, $50 \leq r < 75$ kpc, $75 \leq r < 100$ kpc and $100 \leq r < 200$ kpc. For each particle in a shell, we determine when it was accreted by the main progenitor of the galaxy starting from redshift $z = 2.4$ or 11 Gyr ago. Particles may come from accreted satellites or from the "field". "Field" particles are those which did not belong to any bound structure before becoming part of the galaxy. Because of our resolution limit, field particles may also come from halos with less than 10 particles, i.e. with mass smaller than $8.66 \times 10^5\,{\rm M}_\odot$. The accretion time for particles in a subhalo is defined to be the time of accretion of this subhalo. In practice, we say that a subhalo $H_{\rm sub}$ identified at redshift z has been accreted by the main progenitor $H_{\rm main}$ at redshift z', if at least half of the particles of $H_{\rm sub}$ are contained within $H_{\rm main}$ at z', as well as the most bound particle of $H_{\rm sub}$. For a particle from the field, the time of accretion is simply defined as the earliest time at which this particle has become a member of the main progenitor of the galaxy, as determined by our FOF algorithm.

In Figure 3 we show the fraction of mass accreted (normalised to the present mass) for each shell as a function of the initial mass of the accreted satellite and for three different redshift bins. We divide the analysis into the mass already present at redshift $z = 2.4$ (shown in dark grey); that accreted between $z = 2.4$ and $z = 0.83$ (light grey); and between $z = 0.83$ and the present day (black).

The first panel of Figure 3 shows that the formation time of the inner galaxy is strongly biased towards high redshifts, with more than 60% of the mass already present at $z = 2.4$. We also note that late accretion does not play any role in building up the inner galaxy. Subhalos with masses smaller than $10^7\,{\rm M}_\odot$ accreted at late times do not make up more than 10^{-3} of the total mass in the innermost shell. This has implications for dark-matter detection experiments, since it implies that recently accreted tiny subhalos with very high phase-space density do not contribute enough to the Solar neighbourhood to have a significant effect on the expected signal, in contrast to the suggestion in [37]. The only way such small subhalos could make it to the vicinity of the Sun would be by being accreted first by a large halo, which at some later redshift has a major merger with the main progenitor of the Galaxy. We will quantify how likely this may be in the next section.

Figure 3 also shows that small accreted subhalos tend to deposit most of their mass at large distances. In these outer regions, the contribution of heavy subhalos is of the same order of magnitude as that from the smaller satellites. The difference in the final debris distribution from massive subhalos and from lighter ones is due to dynamical friction; very massive satellites can sink to the centre of the galaxy in short timescales, which enables them to deposit a good fraction of their mass in the central regions. A large fraction (about 20%) of the mass in the

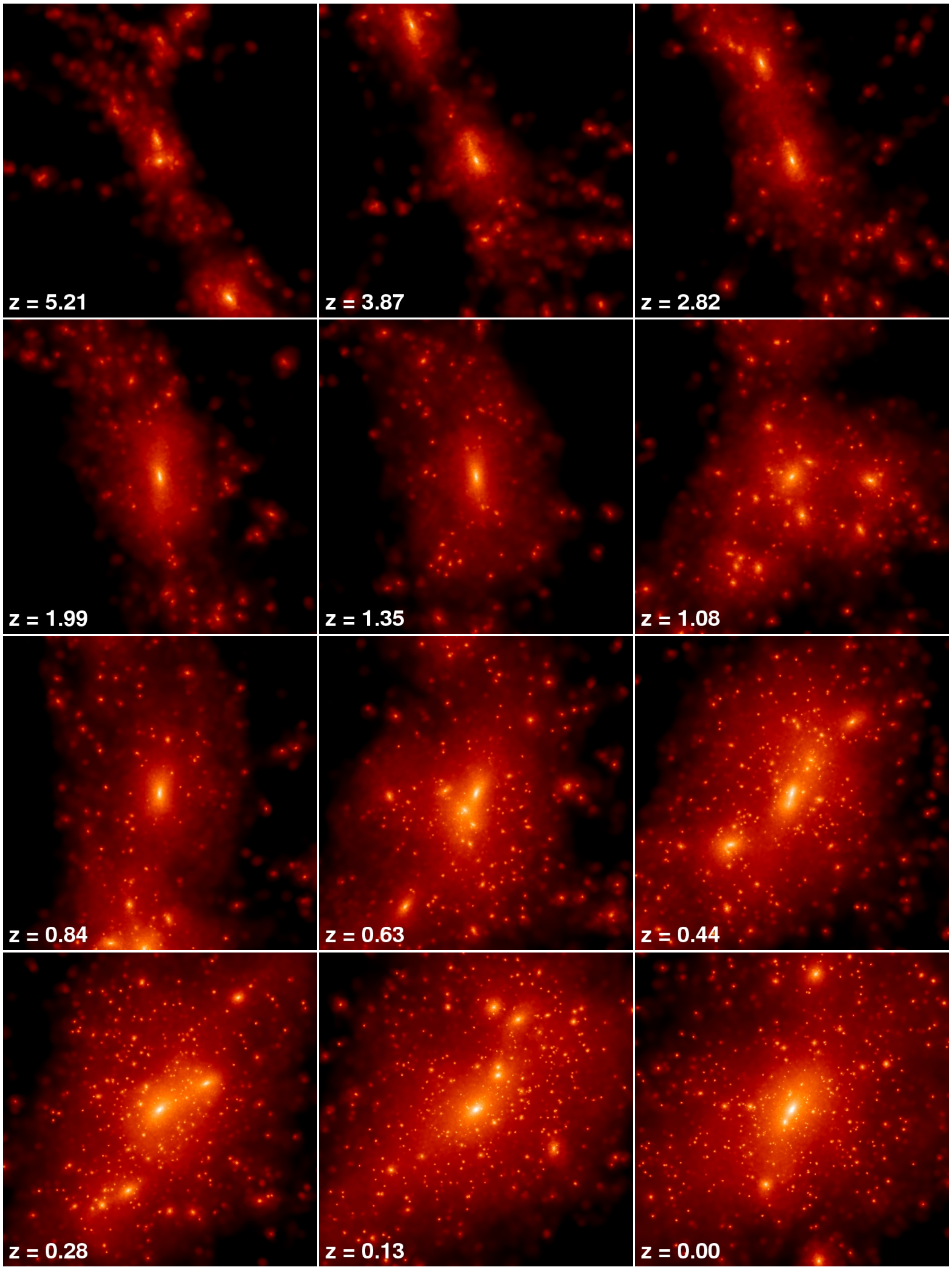

FIG. 1: Snapshots of the growth of the dark-matter halo in our simulation. Each panel shows the projected mass density in a box of side length 5.0 Mpc/h in the original cluster units, which correspond to 778 kpc in the scaled units used throughout the paper. The panels are centred on the main progenitor of the dark-matter halo at that time. The first panel corresponds to 12.7 Gyr ago, and the last panel to the present time. Note how the halo grows through the merging and accretion of smaller units.

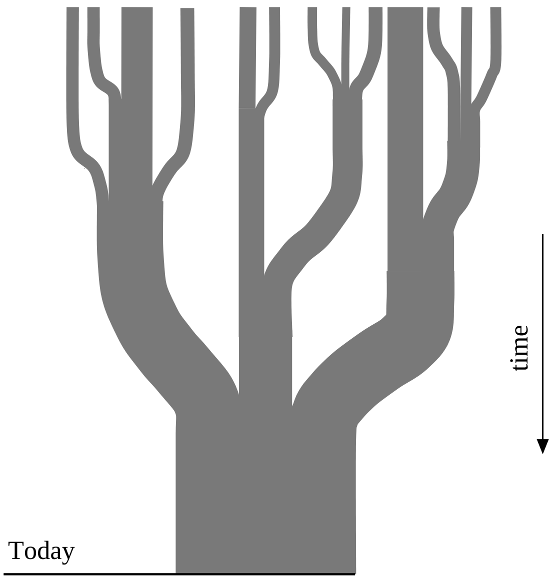

FIG. 2: Schematic representation of a "merger tree" showing the growth of a halo in time. Time increases from top to bottom, and the widths of the branches are proportional to the masses of the progenitor halos (based on [34]).

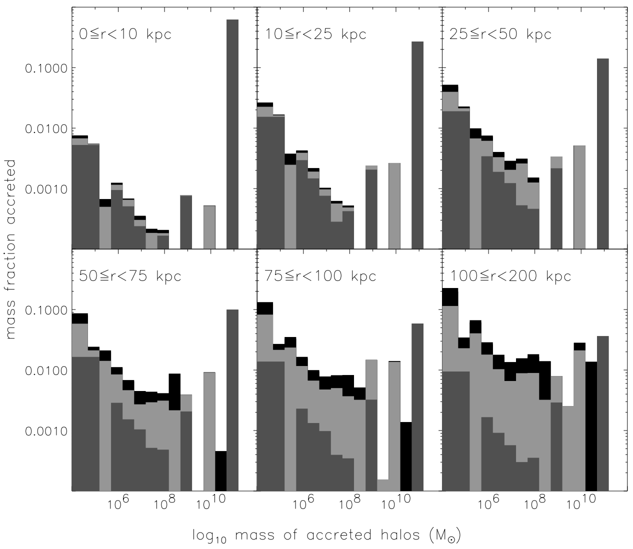

FIG. 3: The panels show the accreted mass fraction (normalised to the present-day mass) as a function of the initial mass of the satellite halo for spherical shells around the galaxy centre. The different colours correspond to the fraction of mass accreted at different redshifts. Dark grey corresponds to the mass already in place at $z = 2.4$; light grey to mass accreted between $z = 2.4$ and $z = 0.83$; and black to that accreted between $z = 0.83$ and the present day.

outskirts comes from field particles (as shown in the last panel of Fig. 3), strongly contrasting with the 0.7% seen for the innermost shell.

Finally we remark that whereas the formation of the inner galaxy is strongly skewed to high redshifts, the outer regions grow much more gradually in time, with accretion still being important at late times.

2. The Solar neighbourhood

We now focus on the "Solar neighbourhood", and analyse the region: 7 kpc $< r <$ 9 kpc. Proceeding as before, we determine the origin of each particle in this spherical shell, and when it was added to the galaxy halo. The growth of mass can take place through mergers or accretion of subhalos, or through a smooth accretion due to the progressive incorporation of field particles.

In the top panel of Figure 4 we show the mass accreted at a given time (to be more precise between two consecutive outputs) $f_m(t)$ normalised to the total present-day mass in the spherical shell 7 kpc $< r <$ 9 kpc. We also show the mass accreted for the whole galaxy halo (thus for $r < r_{\rm vir}$) as a function of time. We thus confirm that all the mergers that contributed a substantial amount of mass to the "Solar neighbourhood" took place quite early. Mergers at late times contributed a relatively large amount of mass to the galaxy halo, but deposited most of this mass in the outer regions of the galaxy.

Particles accreted in the past Gyr, do not account for more than about 10^{-3} of the total present number of particles near the Sun. The influence of streams from such recently accreted material on the velocity distribution function near the Sun will thus be relatively small, and may dominate only the high energy tail of the distribution function.

The lower panel in Figure 4 shows the growth of mass ($F_m(t) = \int_0^t f_m(t')\mathrm{d}t'$) as a function of time. We see that more than 50% of the mass that ends up in the "Solar neighbourhood" today was already in place 11 Gyr ago, and about 90% 10 Gyr ago. Of course, this depends on the specific merger history of this halo, since the large increase of mass observed at $t = 4$ Gyr is due to a major merger taking place at the time. However, we also notice that after $t = 7$ Gyr, there is almost no increase of mass in the vicinity of the "Sun". The large contrast with the gradual mass growth of the halo as a whole can be clearly perceived from this figure.

B. Spatial distribution in the Solar neighbourhood

One of the critical issues in understanding the outcome of the various dark-matter experiments consists in characterising the expected signal. As discussed in the introduction, of fundamental importance is to know whether the distribution of particles in the vicinity of the Sun is smooth or might be dominated by a just a few streams

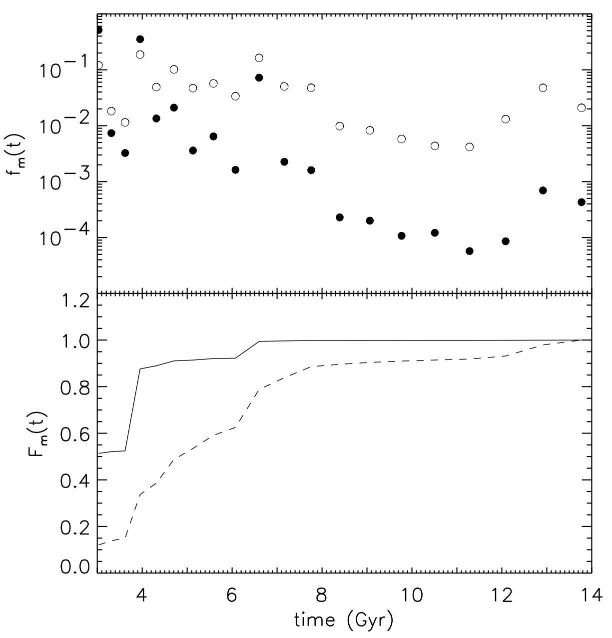

FIG. 4: Filled circles in the top panel show the growth of mass in the "Solar neighbourhood" normalised to the mass present at $z = 0$. Open circles correspond to the growth of mass of the whole galaxy halo. The bottom panel shows to the cumulative growth of mass. Note that 85% of the mass in the Solar neighbourhood was already in place 10 Gyr ago. For the whole galaxy halo (dashed curve), this did not happen until 6 Gyr ago.

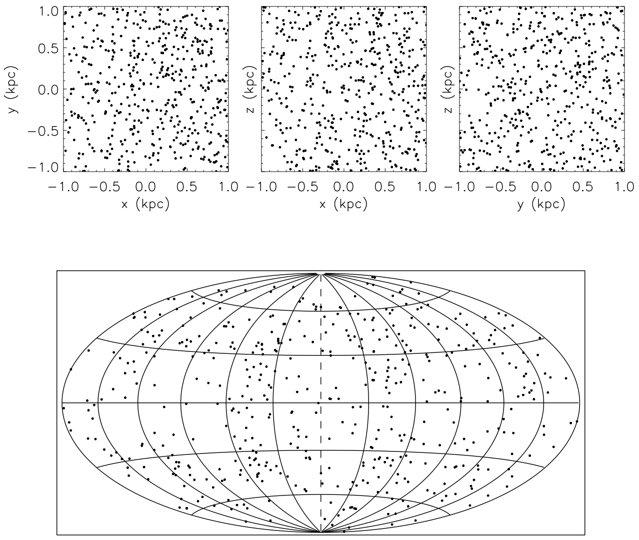

FIG. 5: The top panels show the spatial distribution of particles inside a 2 kpc on a side volume located at 8 kpc from the galaxy centre, i.e. this volume is centred on the "Sun". There are 474 particles in this box. The bottom panel shows their distribution on the sky.

or even bound lumps (e.g. [37]). Below we shall describe the velocity distribution of particles that end up in this region of the galaxy halo. Here we focus on their spatial properties.

In Figure 5 we plot the positions of all particles inside a cubic volume of 2 kpc on a side, located 8 kpc from the "Milky Way" centre, which we assume is the distance between the Sun and the Galactic centre. Because the dark halo is triaxial, although almost prolate (the axes ratios are $I_1 : I_2 : I_3 = 0.65 : 0.71 : 1$), we assume the Galactic disk to be perpendicular to the major axis of the halo. The spatial distribution of particles inside this representative volume is extremely smooth, as shown in Figure 5. This is mostly due to the fact that the material that ends up in the inner galaxy mostly comes from a few very massive halos. The very short dynamical timescales in this region of the galaxy are also responsible for the very rapid and efficient mixing, after which there remains very little or no spatial information on their origin.

1. *The properties of the halos that contribute to the Solar neighbourhood*

To determine the characteristics of the halos that have contributed matter to the Solar neighbourhood, we focus on the spherical shell: 7 kpc $< r <$ 9 kpc. As in Sec.III A 2, we identify the origin of the particles that are located in this shell at the present time. We group the parent satellites according to their initial mass in logarithmically spaced bins of width $dlogM = 0.5$ starting from $10^{5.5}\,\mathrm{M}_\odot$ to $10^{12}\,\mathrm{M}_\odot$. We estimate the contribution from halos identified at three different redshifts. Either such halos are directly accreted by the galaxy, or they are accreted by another more massive subhalo, which eventually merges with the galaxy.

In the left panel of Figure 6 we show the contribution of matter to the spherical shell normalised to the present mass in the shell. Thus we see that a large fraction of the mass in this shell comes from the most massive halos identified at $z = 2.4$, and very little from field particles (as was also shown in Figure 3). For higher redshifts the largest contribution tends to come from smaller satellites, which is just a consequence of the fact that the heaviest halos have not yet collapsed at these redshifts. For sufficiently high redshift, the field particles (i.e. from unresolved halos) are the largest contributor to the mass present today in the Solar neighbourhood.

Just a few individual halos contribute to the largest mass bins. However, for the small mass bins, the number of halos contributing within a given bin actually increases dramatically, as shown in the right panel of Figure 6. The large fraction of the mass in the spherical shell 7 kpc $< r <$ 9 kpc that comes from halos with masses M in the range $10^{5.5} - 10^6\,\mathrm{M}_\odot$ for $z \sim 10$, thus originates in a large number of small independent halos.

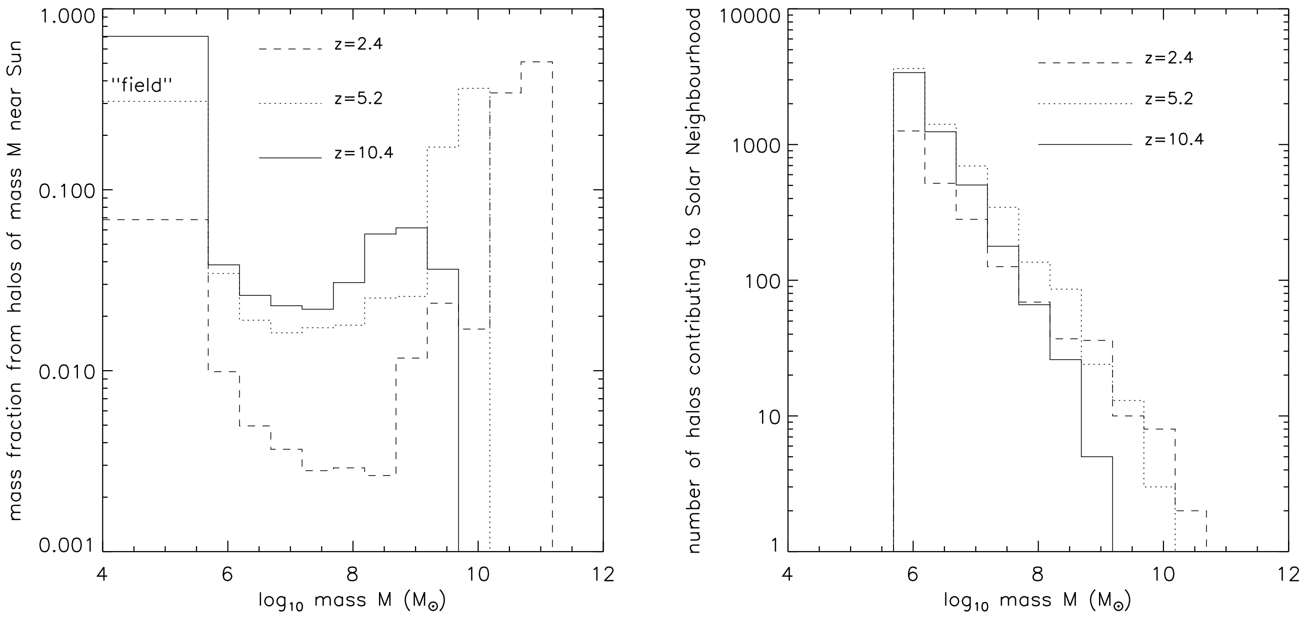

FIG. 6: The left panel shows the fraction of mass in a shell around the "solar" radius coming from halos identified at three different redshifts, normalised to the present mass in the shell. The first bin shows the contribution of field particles at the different redshifts, which end up in the "Solar neighbourhood". By $z = 10.4$ not many massive halos have yet collapsed, and almost all particles come from the field. However, by $z = 2.4$, most of these field particles are found in halos. The largest contribution to mass in the vicinity of the Sun comes from halos heavier than $10^{10}\,\mathrm{M}_\odot$. The right panel shows the number of contributing halos in the different mass bins.

2. Are there any bound subhalos in the Solar neighbourhood?

There have been recent suggestions in the literature that there could be a population of very tiny subhalos orbiting in the Solar neighbourhood [37]. These subhalos which collapsed at very high redshift, might have sufficiently large densities to survive almost intact until the present day. If this picture were correct, their presence would produce a signal on dark-matter detectors that would be very different from that of a Gaussian distribution coming from a smooth halo.

Figure 6 shows that the contribution of mass from halos of $10^{5.5} - 10^6\,\mathrm{M}_\odot$ is not negligible, ranging from 0.9% for halos identified at $z = 2.4$ to 4% for those identified at $z = 10.4$. However, none of these halos has managed to survive bound in our simulations, and so the mass they have contributed is in a smooth component at the present time.

However we also need to quantify the probability that some of the mass actually comes from bound subhalos below our resolution limit. To tackle this problem we need to estimate the fraction of the mass in such subhalos which remained bound until the present day with respect to the total mass of the galaxy. We shall do so using all subhalos orbiting within the virial radius of the galaxy today. These subhalos are mostly found in the outskirts of the galaxy, where their survival times are longer due to the smaller galactic tidal forces.

The subhalo mass function dN/dM gives the number of satellites of the galaxy halo with mass in $[M, M + dM]$. With a sophisticated subhalo finder it is possible to determine dN/dM for our simulated halo at the present time [30]. Figure 7 shows that the number of subhalos in a given mass bin can be well fit by a power law:

$$\frac{dN}{dM} = 1.45 \times 10^{-4} \frac{h}{\mathrm{M}_\odot} \left[\frac{M}{10^7\,\mathrm{M}_\odot h^{-1}} \right]^{-1.73} . \qquad (1)$$

Although the total number of halos with masses smaller than M diverges, the total mass in these halos is a well-defined and finite quantity

$$M_T(< M) = \int_0^M \frac{dN}{dM'} M' dM'.$$

Thus

$$M_T(< M) = 5.29 \times 10^{10} \left[\frac{M}{10^7\,\mathrm{M}_\odot h^{-1}} \right]^{0.27} \qquad (2)$$

in $\mathrm{M}_\odot h^{-1}$. Since the total mass of the galaxy halo in our simulation is $M_{\rm host} = 1.2 \times 10^{12}\,\mathrm{M}_\odot h^{-1}$, the fraction of mass contained in subhalos of mass smaller than M is $p(< M) = M_T(< M)/M_{\rm host}$:

$$p(< M) = 4.4 \times 10^{-2} \left[\frac{M}{10^7\,\mathrm{M}_\odot h^{-1}} \right]^{0.27} . \qquad (3)$$

Thus for example, for the whole galaxy halo the fraction of mass in bound satellites smaller than $10^7\,\mathrm{M}_\odot h^{-1}$ at

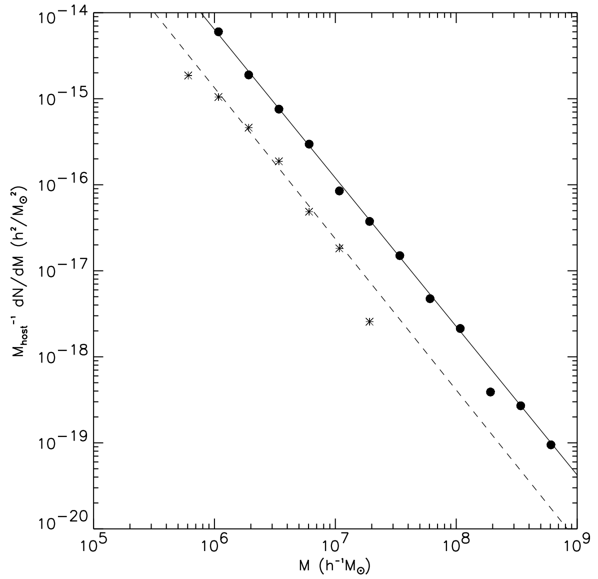

FIG. 7: Differential satellite mass function $M_{\rm host}^{-1} dN/dM$ at redshift $z = 0$ normalised to the mass of the host halo. The solid circles correspond to the whole population of satellites, while the asterisks only to those located in the inner 30 kpc. In the latter case $M_{\rm host}$ is the mass within this spherical region. The straight line corresponds to $\log dN/dM = a + b \log M$, showing that the differential mass function is very well fit by a power law.

the present time is 4.4×10^{-2}. This overestimates the fraction of mass in subhalos orbiting the inner galaxy, since the spatial distribution of subhalos is skewed towards large distances from the galaxy centre, where tidal forces are weaker. For example, if we estimate $p(< M)$ only from subhalos within 30 kpc from the galaxy centre, we find that the fraction of mass in bound satellites smaller than $10^7\,\mathrm{M}_\odot h^{-1}$ is 9.7×10^{-3}, a factor of 5 smaller than previously found. We may conclude that at most about 1 out of one hundred events detected in any dark-matter experiment are expected to come from particles in subhalos with mass below $10^7\,\mathrm{M}_\odot h^{-1}$.

C. Kinematics in the Solar neighbourhood

In Figure 8 we plot the velocities of particles inside a cubic volume of 2 kpc on a side, located at 8 kpc from the "Milky Way" centre. (The same volume as in Figure 5.) We identify with different colours and symbols particles that belonged to the same halo at $z = 2.4$. At this redshift, which corresponds to 11 Gyr ago, we find 252003 halos with at least 10 particles in our simulation. In the box shown in this figure, there are 474 particles which come from 39 different halos; only 3 contribute with more than ten particles. These three halos comprise the main progenitor of the galaxy (i.e. the trunk in Figure 2) and the two most massive halos that merged with the galaxy (see Figure 4. We do not expect all particles of the same colour to be clustered in a single massive stream, since each individual halo is predicted to have given rise to many streams in the Solar neighbourhood [27, 41]. For example, the sixteen particles originating in the third most massive halo (3% of the particles in this volume) are distributed in ten different streams. Therefore, it is not surprising that it is difficult to distinguish streams in this figure. The total number of particles inside this box is too small to populate each expected stream with more than one or two particles.

1. The velocity distribution function

Turning to a larger volume of 4 kpc on a side, allows us to increase the number of particles by roughly a factor of 8. In Figure 9 we plot the velocity distribution function in such a box in the vicinity of the "Sun". The left and right panels show the differential and cumulative velocity distributions, respectively. We also show how these distributions compare to a multivariate Gaussian with the same velocity ellipsoid as the data. Although slight differences are visible, it is hard to distinguish the two distributions from one another without making a detailed statistical comparison.

2. The fastest moving particles

In Figure 10 we show the velocities of particles located in the same 4 kpc on a side box of Fig. 9. We also note here that their velocity distribution is relatively smooth. However, if we focus on the highest energy particles this seems no longer to be the case, as shown by the particles highlighted in grey. The 1% fastest moving particles are strongly clumped. Most of this signal comes from a halo of mass $1.94 \times 10^{10}\,\mathrm{M}_\odot$ that merged with the galaxy at $z \sim 1$. Figure 11 shows the directions of motion of all particles in the box, where we again highlight the fastest moving ones. Their distribution is clearly anisotropic.

3. The velocity correlation function

To quantify the deviations from a smooth Gaussian distribution due to the velocity substructure present in a volume in the Solar neighbourhood, we compute the correlation function in velocity space. We define the (averaged) velocity correlation function $\langle \xi \rangle$ as

$$\langle \xi \rangle = \frac{\langle DD \rangle}{\langle RR \rangle} - 1 \tag{4}$$

(e.g. [40]) where $\langle DD \rangle$ is the number of pairs of particles in our simulation with velocity difference less than a given

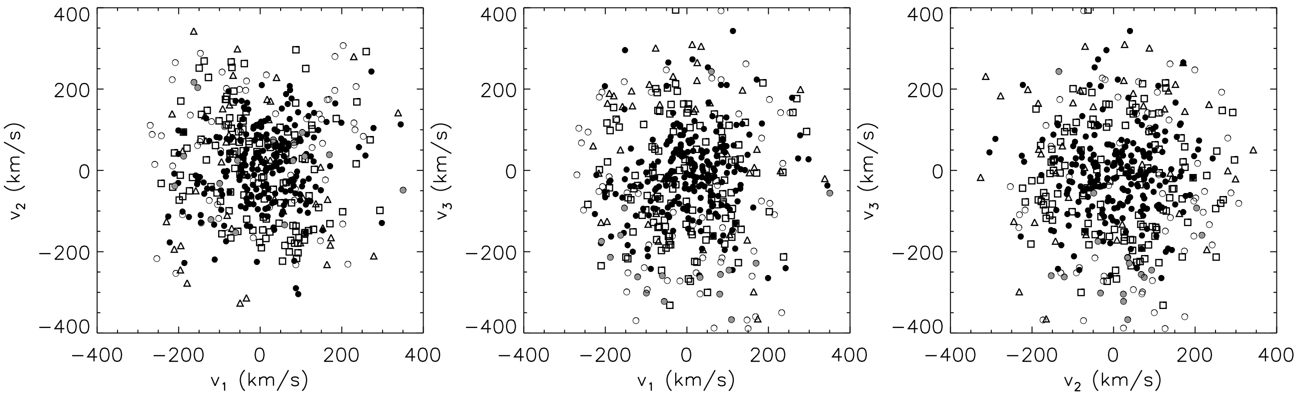

FIG. 8: Principal axes projections of the velocities of particles located in a box of 2 kpc on a side on the "Solar" circle, where all quantities have been scaled to the "Milky Way halo" as described in the text. There are 474 particles in this box. The different colours and symbols are used here to indicate particles originating in the same halo identified 11 Gyr ago. Open circles correspond to particles from halos which do not contribute substantially to this volume. Black filled circles are particles from the main progenitor identified at this redshift (226 particles, i.e. 47%). Open triangles correspond to "field" particles, i.e. not associated to any halo 11 Gyr ago (42 particles, i.e. 9%). The squares (129 particles, i.e. 27%) correspond to the second most massive halo identified at this time, which merged with the galaxy about 10 Gyr ago. The light grey circles (16 particles, 3%) are for the third most massive halo, which merged with the galaxy about 7 Gyr ago. These events are clearly visible in Figure 4, as having contributed most of the mass in the "Solar neighbourhood" in the history of the galaxy.

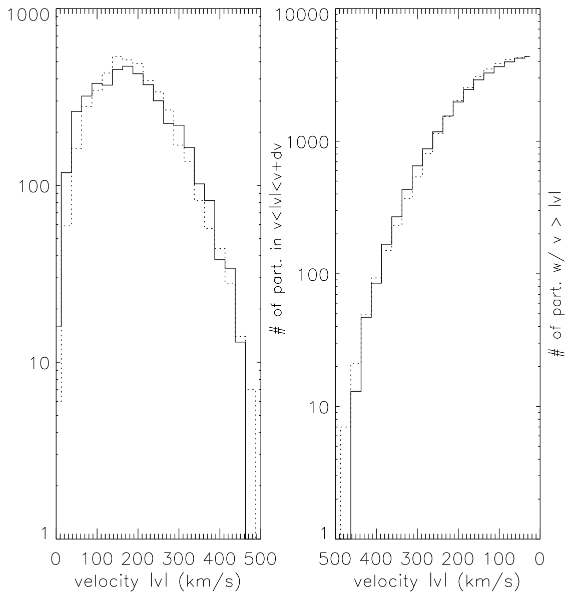

FIG. 9: For particles located in a box of 4 kpc on a side at the "Solar" radius, we plot the differential (left) and the cumulative (right) velocity distributions (solid histograms). The dotted histograms correspond to the expected distribution for a multivariate Gaussian with the same velocity ellipsoid and number of points as the data. The main differences are that the actual distribution of velocities appears to be broader and with a sharper cutoff than the Gaussian, and it is slightly less peaked.

value, i.e.

$$\langle DD\rangle = \sum \text{pairs of particles } i,j \text{ with } |\mathbf{v}_i - \mathbf{v}_j| < \Delta. \tag{5}$$

$\langle RR\rangle$ is defined analogously for the same number of random points. We estimate the error in $\langle\xi\rangle$ as

$$\Delta_{\langle\xi\rangle} = \frac{1+\langle\xi\rangle}{\sqrt{\langle DD\rangle}}. \tag{6}$$

We compare the motions of particles located in the box of Figures 9, 10 and 11 with those expected from a smooth Gaussian distribution. We generate $N_{\rm real} = 10$ different Monte Carlo simulations with the same velocity dispersion tensor and number of points as observed in this box located in the vicinity of the Sun. We compute $\langle\xi\rangle$ as in Eq. (4), with

$$\langle RR\rangle = \frac{\sum_{i=1}^{N_{\rm real}} \langle RR\rangle_i}{N_{\rm real}}, \tag{7}$$

where the sum is over the $N_{\rm real}$ different Monte Carlo realizations. Thus $\langle RR\rangle$ is the number of pairs of random deviates averaged over the ten Monte Carlo realizations. Figure 12 shows that there is a small, but statistically significant, excess of particles with similar velocities (i.e. below 100 km s^{-1}) with respect to what would be expected for a multivariate Gaussian distribution. However if we focus on the 1% fastest moving particles, the excess of pairs of particles with similar velocities is very noticeable, and is a clear indication of the streams visible in Fig. 10. Analysis performed with the 5% fastest moving particles still shows a significant deviation from a multivariate Gaussian, albeit of smaller amplitude. For the 10% fastest moving particles, the deviation is as large as

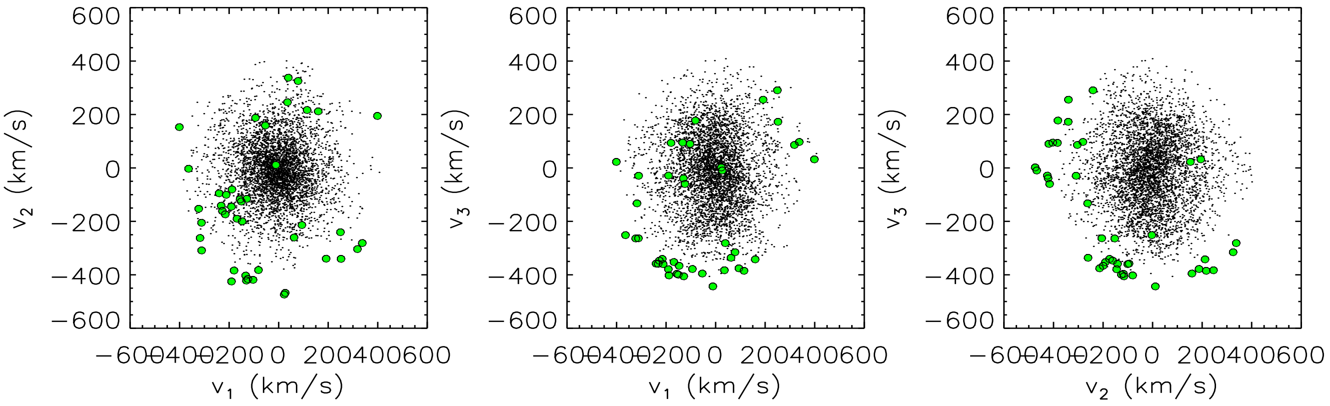

FIG. 10: Principal axes projections of the velocities of particles located in the same box of Fig. 9. Of the 4362 particles present in this volume, we highlighted the 1% fastest. The velocity dispersions along the principal axes are $\sigma_1 = 111.2$ km s^{-1}, $\sigma_2 = 120.1$ km s^{-1}, and $\sigma_3 = 141.4$ km s^{-1}. The lump with $v_1 \sim -185$ km s^{-1}, $v_2 \sim -140$ km s^{-1}and $v_3 \sim -370$ km s^{-1}corresponds to a halo of 1.94×10^{10} M$_\odot$ identified at $z = 2.4$, and accreted at $z = 1$, or 8.2 Gyr ago.

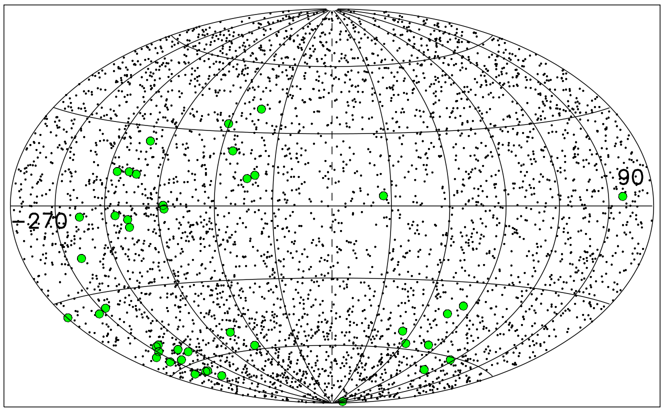

FIG. 11: This plot shows the directions of motion of the same particles discussed in Figs. 9 and 10. We highlight in grey the 1% fastest moving particles. The position of a particle in the plot is given by the spherical angular coordinates of its velocity vector, e.g. $v_1 = v \cos\phi \cos\theta$, where θ is the latitude and ϕ the longitude.

that observed for the full data set, and would thus only be visible with a large number of detection events, i.e. of at least a few thousand dark-matter particles.

Although the results presented here correspond to the analysis of just one box in the "Solar neighbourhood" the features observed here are representative of what is seen for other similar volumes in this region of the galaxy.

IV. DISCUSSION

The build up of dark-matter halos in a hierarchical universe is a very nonlinear process, which happens through the merging and accretion of smaller subunits. The dominant dynamical processes at work are tidal stripping, by which a satellite halo progressively loses its mass, and phase-mixing by which this mass is progressively strung out along streams. As an example we briefly discuss a halo of 4.3×10^{10} M$_\odot$ accreted at $z = 1.8$ ($t = 3.62$ Gyr), and the mass lost between $z = 0.13$ and $z = 0.06$ ($t = 12.08$ and $t = 12.91$ Gyr). In Figure 13 we show the distribution of particles lost in this redshift range, in a 2–dimensional projection (r, v_r) of phase-space. In the left panel we show their distribution just after they were released from their parent satellite. The right panel shows that what was initially a relatively coherent set of particles with similar motions, has by the present time spread out into four different streams which are seen to overlap in space. Note that this happened in less than 1.7 Gyr, which shows how short the mixing timescales are in the inner galaxy.

The density in a stream decreases in time, as the particles spread out along the orbit of their progenitor system. Because the orbit defines a 3–dimensional volume (a doughnut shaped volume defined by the orbital turning points), the density in a stream will decrease as $(t/t_{\rm orb})^{-3}$ [27]. Thus, extrapolating the result obtained for the material shown in Fig. 13 – the formation of 4 streams in 1.7 Gyr–, and noting the very early build up of the galaxy halo (as demonstrated in Sec. III A 2), we estimate that at least $4 \times (0.7\,{\rm Gyr}/0.35\,{\rm Gyr})^3 \times (10\,{\rm Gyr}/1.7\,{\rm Gyr})^3 \sim 6500$ dark streams should be present in the Solar neighbourhood (a detailed careful analysis, taking also into account other halos, shows that this number should be even larger [41]). Here we used that the orbital periods of particles in Fig. 13 are of the order of 0.7 Gyr, while the median for particles near the Sun is closer to 0.35 Gyr.

We note here that some authors [24, 26] have assumed that the density decrease in a stream is slower in time (linear or quadratic), from which they (incorrectly) deduce that the streams should have much higher densities. These works then argue that streams can strongly affect the signal detected for the flux of dark-matter particles going through the Earth. We have just shown this is not the case.

These results also apply to the density contrast in caus-

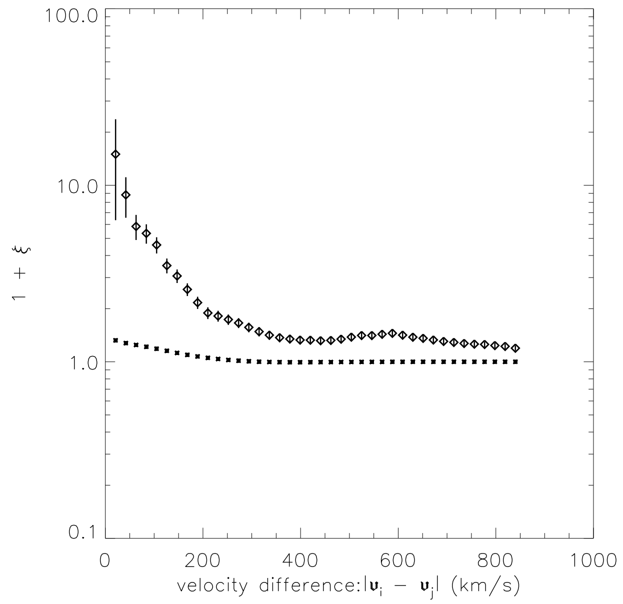

FIG. 12: For the same box as in Figures 9, 10 and 11, we plot the "(averaged) velocity correlation function" $\langle\xi\rangle$. It is defined as the number of neighbours with velocity difference less than a given value compared to what is expected for random deviates. In this case the random deviates are drawn from a multivariate Gaussian with the same number of particles and velocity dispersion tensor as the data. Asterisks correspond to $\langle\xi\rangle$ over all the particles in the box, whereas diamonds to the 1% fastest moving particles. Both for the full data set and for the fastest moving particles there is a signal at small velocity differences, indicative of the presence of streams. This signal is clearly much stronger for the subset of most energetic particles. The error bars are based on Poissonian counts.

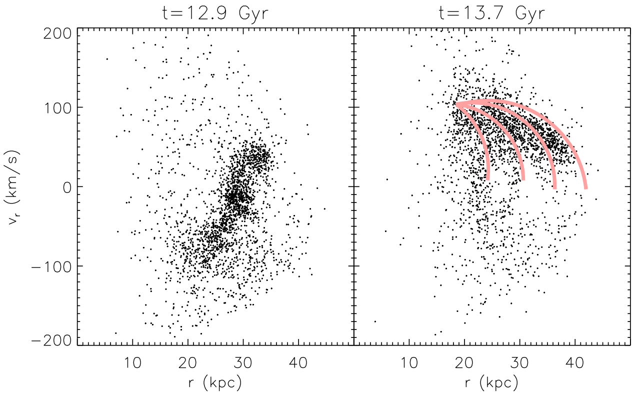

FIG. 13: Here we show the phase-space projection (r, v_r) for particles lost from a halo between $z = 0.13$ and $z = 0.06$ (between 12.1 and 12.9 Gyr). The left panel shows their distribution close to when they were released. The right panel shows their present day distribution. The multiple streams were produced in the lapse of at most 1.7 Gyr. The grey curves have been added to highlight the location of these streams in the diagram.

tic surfaces or rings, expected to form at the orbital turning points. We note here that the proposed large effect associated with sheets of particles falling in for the first, second or third time is not observed in our simulations. This is *not* due to our finite resolution (as suggested by [42]), but due to the fact that the formation time of the inner halo is so strongly biased to high redshifts. Since particles which orbit the Solar neighbourhood have orbital periods of the order of 0.35 Gyr, and the inner galaxy was already in place 10 Gyr ago, this implies that the density of these caustic structures should be of the order of $(10\ \mathrm{Gyr}/0.35\ \mathrm{Gyr})^{-3} \sim 4 \times 10^{-5}$ times smaller today. For these reasons structures such as caustic rings or surfaces will likely have no effect on the signal that dark-matter experiments will detect.

Recent analytic work [25] has focused on the effect of recently accreted material on the velocity distribution function near the Sun. As these authors discuss, such material will mostly dominate the high energy tail of the velocity distribution, and provide a non-Gaussian and perhaps more easily detectable feature in the spectrum of particles that go through the Earth. Although we reach a similar conclusion in Sec.C.2, we do not agree on the magnitude of this effect. In particular, we find that the density of streams from such recently accreted material is a factor of ten smaller than has been estimated in [25]. Probable causes for this discrepancy can be perhaps be attributed to the different orbital distributions of the accreted lumps (provided *ab initio* in our simulations, and assumed to have a particular form in [25]); and in the different methods used to measure the density of a stream (total density of material from an accreted halo versus density of individual streams).

Although our simulation represents the formation of a cluster halo, rather than that of a galaxy, and it is only one possible realization of the formation of a dark-matter halo, we believe the conclusions we have reached are robust. For example, the mass growth history of this particular halo is consistent with that of the Milky Way: most of the mass was already in place in the cluster halo 10 Gyr ago, in good agreement with the age of the oldest stars in the Milky Way disk. High resolution simulations by other authors have shown that galaxy and cluster sized halos grow in statistically similar ways and that our particular halo is not unusual [36] (see also [44]). Also, the properties of the velocity distribution of dark-matter in the Solar Neighbourhood are in good agreement with the observed kinematics of halo stars [43]. Moreover, the characteristics of the streams in our simulation, such as their low densities and large number, are consistent with the simple analytic estimates discussed above. Work along the lines of [25] can provide further insight on how much variation one may expect to find on a halo-to-halo basis.

V. CONCLUSIONS

We analysed a high resolution simulation of the formation of a cluster in a ΛCDM cosmology. By scaling it down to a galaxy size halo (by the ratio of the maximum circular velocities) we were able to make predictions for the expected dark-matter distribution near the Sun.

Our results indicate that direct detection experiments may quite safely assume that the distribution of dark-matter particles in the Solar neighbourhood is well represented by a multivariate Gaussian. We find that none of the streams present in any of the volumes at the Sun's distance from the Galactic centre dominate their local distribution. The mean density of an individual stream is typically 0.3% that of the local dark-matter distribution (deduced from the number of particles in the rather dense stream shown in Figure 10). These small values are due to the fact that most of the streams in the inner galaxy come from a few massive halos that merged at high redshift to build up the object we see today. These large halos mix extremely quickly and therefore give rise to low density structures. Strong density enhancements such as those predicted in [24, 42] are extremely unlikely in the inner Galaxy. Our simulation also shows that we should not expect to find dense, recently formed streams near the Sun, since the last accretion contributing matter to the Solar neighbourhood typically took place about 1 Gyr ago, and provides only $\sim 10^{-4}$ of the total mass in this region. Moreover, we find that fewer than 1% of the local dark-matter particles could be part of small dense subhalos which have survived intact within the larger halo of the Milky Way. It is therefore unlikely that an individual halo with these characteristics will dominate the signal in direct detection experiments.

Direct detection experiments which are sensitive to the direction of motion of the fastest moving dark-matter particles may discover a direct indication of the hierarchical growth of our Galaxy's halo. The expected signal for these fastest moving particles is highly anisotropic, and could be eventually be used, not just to determine the nature of the dark-matter, but also to recover, at least partially, the recent merging history of the Milky Way.

We thank Ben Moore and Leo Stodolsky for useful discussions which triggered many of the ideas discussed here; Uros Seljak and Anne Green for helping us improve the manuscript. AH wishes to thank Joke for being a continuous source of inspiration.

[1] F. Zwicky, Helv. Phys. Acta **6** 110 (1933).
[2] S. Smith, Astrophys. J. **83** 23 (1936).
[3] V. Rubin & W.K. Ford, Astrophys. J. **159** 379 (1970).
[4] S. Faber & J.S. Gallagher, Ann. Rev. Astron. and Astroph. **17** 135 (1979).
[5] V. Rubin, W.K. Ford & N. Thonnard, Astrophys. J. **238** 471 (1980).
[6] P.J.E. Peebles, Astrophys. J. Lett. **189** 51 (1974).
[7] P.J.E. Peebles, Astrophys. J. Lett. **263** 1 (1982).
[8] G.R. Blumenthal, S.M. Faber, J.R. Primack & M.J. Rees, Nature **311** 517 (1984).
[9] M. Davis, G. Efstathiou, C.S. Frenk & S.D.M. White, Astrophys. J. **292** 371 (1985).
[10] R. Peccei & H.R. Quinn, Phys. Rev. Lett. **38** 1440 (1977).
[11] C. Hagmann *et al.*, Phys. Rev. Lett. **80** 2043 (1998).
[12] I. Ogawa, S. Matsuki & K. Yamamoto, Phys. Rev. D **53** 1740 (1996).
[13] R. Bernabei *et al.* [DAMA Collaboration], Phys. Lett. B **480**, 23 (2000).
[14] R. Abusaidi *et al.* [CDMS Collaboration], Phys. Rev. Lett. **84**, 5699 (2000).
[15] A. Benoit *et al.* [EDELWEISS Collaboration], Phys.Lett. B **513** 15 (2001).
[16] L. Bergström, Rep. Prog. Phys. **63** 793 (2000).
[17] D.N. Spergel, Phys. Rev. D **37** 1353 (1988).
[18] A.K. Drukier, K. Freese & D.N. Spergel, Phys. Rev. D **33** 3495 (1986).
[19] K. Freese, J. Frieman & A. Gould, Phys. Rev. D **37** 3388 (1988).
[20] R. Bernabei *et al.* [DAMA Collaboration], Phys. Lett. B **424** 195 (1998).
[21] P. Ullio & M. Kamionkowski, J. High Energy Phys. **103** 049 (2001).
[22] A.M. Green, Phys. Rev. D **63** 043005 (2001)
[23] N. W. Evans, C. M. Carollo & P. T. de Zeeuw, Mon. Not. R. Astron. Soc. **318** 1131 (2000).
[24] P. Sikivie, Phys. Lett. B **432** 139 (1998).
[25] D. Stiff, L.M. Widrow & J. Frieman, Phys. Rev. D **64** 083516 (2001).
[26] C. Hogan, Phys.Rev. D **64** 063515 (2001).
[27] A. Helmi & S. D. M. White, Mon. Not. R. Astron. Soc. **307** 495 (1999).
[28] A. Helmi, S. D. M. White, P. T. de Zeeuw & H.S. Zhao, Nature **402** 53 (1999).
[29] R. Ibata, G. Gilmore & M. Irwin, Nature **370** 194 (1994).
[30] V. Springel, S.D.M. White, G. Tormen & G. Kauffmann, Mon. Not. R. Astron. Soc. **328** 726 (2001).
[31] V. Springel, N. Yoshida & S.D.M. White, New Astron. **6** 79 (2001).
[32] G. Tormen, F.R. Bouchet & S.D.M. White, Mon. Not. R. Astron. Soc. **286** 865 (1997).
[33] A. Guth, Phys. Rev. D **23** 347 (1981).
[34] C. Lacey & S. Cole, Mon. Not. R. Astron. Soc. **262** 627 (1993).
[35] B. Moore, S. Ghigna, F. Governato, G. Lake, T. Quinn, J. Stadel & P. Tozzi, Astrophys. J. Lett. **524** 19 (1999).
[36] Y.P. Jing, Y. Suto, Astrophys. J. Lett. **529** 69 (2000).
[37] B. Moore, C. Calcaneo-Roldan, J. Stadel, T. Quinn, G. Lake, S. Ghigna & F. Governato, Phys. Rev. D **64** 063508 (2001).
[38] P. Sikivie, I.I. Tkachev & Y. Wang, Phys. Rev. D **56** 1863 (1997).
[39] K. Freese, P. Gondolo & L. Stodolsky, Phys. Rev. D **64** 123502 (2001).
[40] M. Kerscher, I. Szapudi & A. Szalay, Astrophys. J. Lett. **535** 13 (2000).

[41] A. Helmi, S. D. M. White & V. Springel, in preparation.
[42] P. Sikivie, astro-ph/0109296 (2001).
[43] M. Chiba & T. C. Beers, Astron. J. **119** 2843 (2000).
[44] D. Zhao, H. Mo, Y.P. Jing & G. Boerner, astro-ph/0204108 (2002).
[45] This is because $M \propto R^3 \propto V^3$, and thus if $M_f = 2M_i$ then $R_f^3 V_f^3 \propto 4R_i^3 V_i^3$
[46] If initially $\Delta_x \Delta_v$ is the phase-space volume occupied by the satellite, and if Δ'_x is its final volume, then $\Delta'_v = \Delta_v \times \Delta'_x / \Delta_x$, where as discussed above, Δ'_x is the volume given by the orbit, and is much larger than the original volume of the satellite.